Clays and Clay Minerals, Vol. 61, No. 4, 303–318, 2013.

REACTION PATHWAYS OF CLAY MINERALS IN TROPICAL SOILS: INSIGHTS FROM KAOLINITE-SMECTITE SYNTHESIS EXPERIMENTS

PETER C. RYAN[1,2,*] AND F. JAVIER HUERTAS[2]

[1] Geology Department, Middlebury College, Middlebury, Vermont, 05753 USA
[2] Instituto Andaluz de Ciencias de la Tierra (CSIC-Universidad of Granda), 18100 Armilla, Granada, Spain

Abstract—Pedogenic smectite from a young (Holocene) tropical soil was reacted in Al-rich solution at 150ºC for a range of reaction times (3 to 120 days) in order to study mechanisms and rates associated with the transformation of smectite to kaolinite *via* interstratified kaolinite-smectite (K-S). As has been observed in tropical soils, the overall reaction rate is logarithmic, with rapid initial transformation of smectite to K-S with ~50% smectite layers, followed by progressively slower transformation of intermediate K-S to kaolinite-rich K-S and eventually Fe-kaolinite. Sub-micron hexagonal non-Fe-bearing kaolinite forms in the final stage (after 120 days) as a minor mineral in an assemblage dominated by Fe-kaolinite. The pedogenic smectite used as starting material consisted of two end-members, Fe-beidellite and Al-smectite, enabling comparison of reaction pathways. Fe-beidellite transforms to K-S or Fe-kaolinite within 3 days, whereas Al-smectite transforms much more slowly, appearing to reach a maximum rate in intermediate stages. This difference is probably due to hydrolysis of relatively weak Mg−O and Fe−O bonds (relative to Al−O bonds) in Fe-beidellite octahedral sheets, which drives rapid reaction, whereas the driving force behind transformation of Al-smectite is more likely to be related to stripping of tetrahedral sheets which reaches its maximum rate at intermediate stages. Multiple analytical approaches have indicated that Al is rapidly fixed from solution into smectite interlayers within K-S, and that K-S and Fe-kaolinite inherit octahedral Fe and Mg from precursor smectite; as the reaction progresses, octahedral sheets become progressively more Al-rich and Fe and Mg are lost to solution. These results demonstrate that: (1) early-formed pedogenic smectite in tropical soils is expected to transform to kaolinite *via* interstratified K-S; (2) K-S has a strong potential to sequester plant-toxic Al in tropical soil; and (3) the presence in tropical soils of Fe-kaolinites with relatively large cation exchange capacities may be related to inheritance of octahedral sheets from precursor smectite and K-S.

Key Words—Beidellite, Fe-kaolinite, Interstratified, Kaolinite-smectite, Mixed-layer, Pedogenic, Smectite, Soil, Synthesis, Transformation, Tropical.

INTRODUCTION

The occurrence of interstratified kaolinite-smectite (K-S) has been recognized in a few studies of soils from subtropical or tropical climates (*e.g.* Altschuler *et al*., 1963; Delvaux *et al*., 1990; Righi *et al*., 1999; Ryan and Huertas, 2009; Hong *et al*., 2012), but relatively few studies to date have examined mechanisms or rates of the transformation from smectite to kaolinite *via* interstratified K-S (Środoń, 1980; Amouric and Olives, 1998; Dudek *et al*; 2007; Cuadros *et al*., 2009; Ryan and Huertas, 2009), and even fewer have examined the implications of this reaction sequence on soil properties (Delvaux *et al*., 1990; Churchman *et al*., 1994; Ryan and Huertas, 2009; Hong *et al*., 2012). Given the pronounced differences in cation exchange capacity, Al uptake capability, and physical properties (*e.g.* shrink-swell and erosion potential) among end-member smectite and kaolinite as well as various interstratifications of K-S, understanding rates and mechanisms of the transformation of smectite → K-S → kaolinite is a necessary component of predicting soil physical and chemical properties, especially in the tropics where clays commonly make up >60% of soil.

The common paradigm for moist-to-humid tropical soils describes a kaolinite-dominated mineralogy with low concentrations of base cations, low pH (4.5−5.0), and large amounts of exchangeable Al (*e.g.* Vitousek and Sanford, 1986; Quantin *et al*., 1991; Chadwick *et al*., 1999; Etame *et al*., 2009), yet this model applies to only 35% of the tropics. The majority of tropical soils are Inceptisols, Alfisols, Andisols, or Ultisols (NAP, 1982), soils which may contain smectite and/or interstratified K-S, especially in relatively young soils (formed on late Pleistocene or Holocene parent material) (Eswaran and de Coninck, 1971; Kantor and Schwertmann, 1974; Wada *et al*., 1990; Thanachit *et al*., 2006; Ryan and Huertas, 2009). These soils have cation exchange capacities (CEC) that are roughly an order of magnitude greater than kaolinite-dominated Oxisols, and are also characterized by correspondingly low Al toxicity, circum-neutral to only slightly acidic pH, relatively high base cation reserves, and negative surface charge (due to the presence of smectites or related 2:1 clay minerals). With sufficient time in the intense leaching regime associated with most tropical soils, the mineral assemblage evolves to one

* E-mail address of corresponding author:
pryan@middlebury.edu
DOI: 10.1346/CCMN.2013.0610410

dominated by kaolinite and sesquioxides, and soil chemistry becomes characterized by a large amount of available Al, a small base cation content, low pH (Fisher and Ryan, 2006; Ryan and Huertas, 2009), and positive surface charge reflecting the abundance of Al- and Fe-(oxyhydr)oxides (Anda *et al*., 2008).

The purpose of the present study was to investigate reaction mechanisms and rates of the transformation of pedogenic smectite (S) to kaolinite (K) *via* interstratified K-S. Previous research has documented this reaction sequence in a 125 ka tropical soil chronosequence, where $\leqslant$5 ka soils are dominated by smectite, 10−40 ka soils are dominated by K-S, and 125 ka soils are rich in K-S and Fe-kaolinite (Ryan and Huertas, 2009). The reaction of smectite to K-S in this soil sequence, and in apparently all smectite to K-S reactions, occurs on a layer-by-layer basis within crystals *via* stripping of tetrahedral sheets (in response to leaching of Si) and incorporation of Al-hydroxy complexes that transform smectite interlayers to kaolinite octahedral sheets (*e.g.* Środoń, 1980; Delvaux *et al*., 1989; Dudek *et al*., 2007; Cuadros *et al*., 2009; Ryan and Huertas, 2009). The significance of this cell-preserved mechanism (*i.e.* reactions occurring within the framework of a crystal involving localized dissolution to facilitate structural rearrangements) for tropical soils is that it results in K-S and Fe-kaolinite with CEC values that exceed end-member $Al_2Si_2O_5(OH)_4$ kaolinite; furthermore, the presence of 2:1 layers within K-S appears to provide a sink for Al, thus limiting plant-toxic Al in soil solution (*e.g.* Korning *et al*., 1994).

In the current study, the transition of S → K-S → K was studied *via* a series of controlled laboratory experiments designed to examine reaction mechanisms and kinetics. The advantage of controlled laboratory alteration experiments for this type of study is that the same pedogenic smectite sample can be exposed to a range of reaction times, thus allowing examination of reaction rate and mechanism without the influence of variables such as changing parent material composition over time or the deposition of eolian clays into soils. The reaction conditions used in the current study were identical to those employed by Środoń (1980) and Dudek *et al*. (2007) when they examined reaction of Al-rich montmorillonite to K-S, which enables comparison of reactions rates and mechanisms of the relatively Fe-Mg-rich soil smectites studied herein with those of Al-montmorillonites studied by Środoń (1980) and Dudek *et al*. (2007); furthermore, the Al-rich composition of the reaction solution is analogous to Al-rich tropical soil solutions, so the chemical driving force in this experiment is comparable to tropical soils.

MATERIALS AND METHODS

The smectite used as starting material in this study is the dominant pedogenic mineral in a late-Holocene (<5 ka) tropical Inceptisol (Qt4-C5) from Costa Rica (Fisher and Ryan, 2006). Qt4-C5 is the youngest soil in a 125 ka fluvial terrace chronosequence that exhibits the sequential transformation of smectite to: (1) K-S with 60−70% kaolinite layers in 10−40 ka soils; and (2) a mixture of Fe-kaolinite and K-S with 85−90% kaolinite layers in 125 ka soils (Ryan and Huertas, 2009).

For synthesis experiments, four separate Ca-saturated 200 mg portions of the <2 μm fraction of Qt4-C5 were placed in 50 mL Teflon-lined Parr 4744 steel reactors and mixed with 25 mL of a 32 mmol L^{-1} solution of Al. The solution was prepared from $AlCl_3{\cdot}6H_2O$ and distilled water by adding 0.800 mmol of Al (193.16 mg of $AlCl_3{\cdot}6H_2O$) to each 25 mL of distilled water following the protocols of Środoń (1980) and Dudek *et al*. (2007); the pH of the initial solutions was 3.4. Hydrothermal synthesis treatments were performed by heating powder-solution mixtures in an oven at 150ºC and at the corresponding water-vapor pressure (4.8 atm) in a step-wise manner: one 200 mg specimen of Qt4-C5 was reacted for 3 days, a second 200 mg specimen of Qt4-C5 was reacted for 30 days, a third was reacted for 60 days, and a fourth was reacted for 120 days. The concentration of Al in solution and the amount of clay selected for these experiments is the same as used by Dudek *et al*. (2007) and is very similar to the experimental parameters of Środoń (1980) – both of these studies produced interstratified K-S from aluminous smectite, and the present authors wanted to select parameters that allowed for comparison of results. Środoń (1980) and Dudek *et al*. (2007) reacted aluminous montmorillonite for 120 days. The present authors selected a series of reaction times (3, 30, 60, 120 days) for the suites of samples to examine reaction mechanisms and kinetics in smectites that are pedogenic (as opposed to volcanic/hydrothermal) and more Fe-rich than those studied by Środoń (1980) and Dudek *et al*. (2007).

Reactors were cooled quickly at the end of each experiment to prevent the precipitation of silica phases; solids were separated from solutions immediately by centrifugation. Reaction products were Ca saturated by suspending the remaining ~200 mg of <2 μm fraction in a 20 mL solution of 0.5 M $CaCl_2$, sonicating the suspension to disaggregate the clay, and allowing it to equilibrate overnight. After centrifuging to separate solids from solution and pouring off supernatant, this process was repeated again with 0.05 and 0.005 M solutions of $CaCl_2$, pouring off supernatant in each case. The resulting Ca-saturated clays were then subsequently washed three times with deionized water to remove any Ca not electrostatically attracted to mineral particles, and resulting Ca-saturated fractions were dried at 60ºC and ground gently and homogenized for subsequent X-ray diffraction (XRD), transmission electron microscopy-analytical electron microscopy (TEM-AEM), Fourier-transform infrared spectroscopy (FTIR), and differential thermal analysis (DTA).

The XRD analysis was performed on natural specimens and solid reaction products of hydrothermal treatments using a PANalytical X'Pert Pro system operating at 45 kV and 40 mA with an X'Celerator detector, CuKα radiation, a Ni filter, and 0.25º divergence slit. Oriented powders were prepared by pipetting concentrated powder suspensions in deionized water onto glass slides, and oriented mounts were scanned continuously from 3 to 40º2θ (3.5º/min) in air-dried (AD), ethylene glycol-solvated (EG), and heated states (300ºC for 1 h, 400ºC for 2 h, 550ºC for 2 h). The percentage of kaolinite layers in interstratified K-S was calculated by comparing the experimental ethylene-glycol saturated patterns to data in Cradwick and Wilson (1972) and Moore and Reynolds (1997), with an estimated uncertainty of ±5%. The XRD peaks were deconvoluted using *MacDiff* 4.2.5 (Petschick, 2000). Random powder mounts used to examine three-dimensional structures which were prepared from gently ground <2 μm fractions of Ca-saturated powders that were sprinkled onto a zero-background silicon sample holder, cut with a razor blade to enhance random orientation, and coalesced using acetone. These preparations were analyzed from 3 to 70º2θ (1.5º/min) and then from 58 to 65º2θ (0.5º/min) to enhance analysis of the 06,33 region.

The TEM-AEM analyses were performed at the Centro de Instrumentación Científica (CIC) at the Universidad de Granada using a Philips CM-20 electron microscope fitted with an ultrathin window and solid-state Si(Li) detector for energy dispersive X-ray analysis (EDAX). The <2 μm fraction was suspended in pure ethyl alcohol and mounted on Cu grids, and analyses were performed at 200 kV with a 200 nm spot size. Atomic proportions calculated from peak intensities were converted into atomic concentrations using natural mineral standards and quantitative calibration was carried out by the method of Cliff and Lorimer (1975). The percentage of kaolinite layers in interstratified K-S was determined by extrapolation from beidellite and kaolinite end-member compositions. The high degree of variability in end-member composition, especially in the beidellites, produced an uncertainty of 15%.

The FTIR spectra were recorded on a Perkin-Elmer Spectrum One FTIR spectrometer in absorbance mode (4000−400 cm^{-1} range) with a resolution of 4 cm^{-1}. Samples were prepared as KBr pressed pellets by diluting 1 mg of sample in 150 mg of dried KBr. The pellets were heated overnight at 120ºC before analysis.

The DTA-TG (thermogravimetric) analyses were carried out using a Netzsch STA 409EP simultaneous thermal analyzer using 25 mg of sample in an air atmosphere. Al_2O_3 was used as reference material, the temperature range was 25−1020ºC, and the heating rate was 10ºC/min. Temperatures according to dehydration and dehydroxylation reactions were determined using the DTA, TG, and first-derivatives of the TG curves (DTG). The quantities of smectite and kaolinite were quantified by DTA by applying the method of Dudek *et al*. (2006, 2007), where end-member smectite experienced 6% weight loss over the dehydroxylation temperature range of 350−1000ºC and kaolinite lost 14% over the same range. Dehydroxylation weight loss associated with K-S transformations is non-linear, details of which were described by Dudek *et al*. (2006, 2007).

The liquid phase remaining after reaction was analyzed for pH immediately after the solutions had cooled to room temperature, and Al, Ca, K, Mg, Fe, and Si were determined by inductively coupled plasma-atomic emission spectrometry (ICP-AES) at Middlebury College, Vermont, USA. The uncertainty of the pH measurements was ±0.1 units; for ICP-AES analyses, the uncertainty was within 10% of measured values based on analyses of replicates and synthesized standards.

RESULTS

Combined data from XRD, TEM-AEM, DTA-TG, and FTIR indicated that pedogenic smectite (Qt4-C5) transformed sequentially to interstratified K-S with 50% K layers after Stage 1 (3 days), to K-S with 60 to 80% K layers after Stages 2 and 3, and, ultimately (by Stage 4, 120 days), to a mixture of Fe-kaolinite, interstratified K-S with 90−95% K layers, and small amounts of discrete, very fine-grained euhedral kaolinite with end-member $Al_2Si_2O_5(OH)_4$ composition. The reaction rate decayed logarithmically with time, and Fe and Mg were lost from octahedral sheets during the reaction series, consistent with step-wise dissolution of octahedral sheets throughout the reaction sequence. The following sections present data from the different analytical approaches.

XRD

X-ray diffraction patterns (Figure 1) of ethylene-glycol solvated, oriented mounts (<2 μm fraction) of the synthesis sequence revealed the following, starting with pedogenic smectite (Qt4-C5) followed by derived reaction products: Stage 1 (3 days) products contained K-S with ~50% kaolinite layers; Stages 2 and 3 (30−60 days) contained K-S with ~60−80% kaolinite layers; finally, Stage 4 (120 days) products consisted of a very kaolinite-rich assemblage with no XRD evidence of smectite layers remaining in K-S. The shift to an assemblage dominated by kaolinite layers was also indicated in the 060 region where initial Qt4-C5 produced a pair of dominant 060 peaks, one at 1.503 Å, and the other at 1.498 Å, both from smectite; the 1.503 Å peak from Fe-rich smectite (~10% Fe_2O_3) and the 1.498 Å peak from Fe-poor smectite (~4% Fe_2O_3). More details on these two smectite end-members are presented below in the TEM-AEM section. The 1.503 Å Fe-smectite peak effectively disappeared by

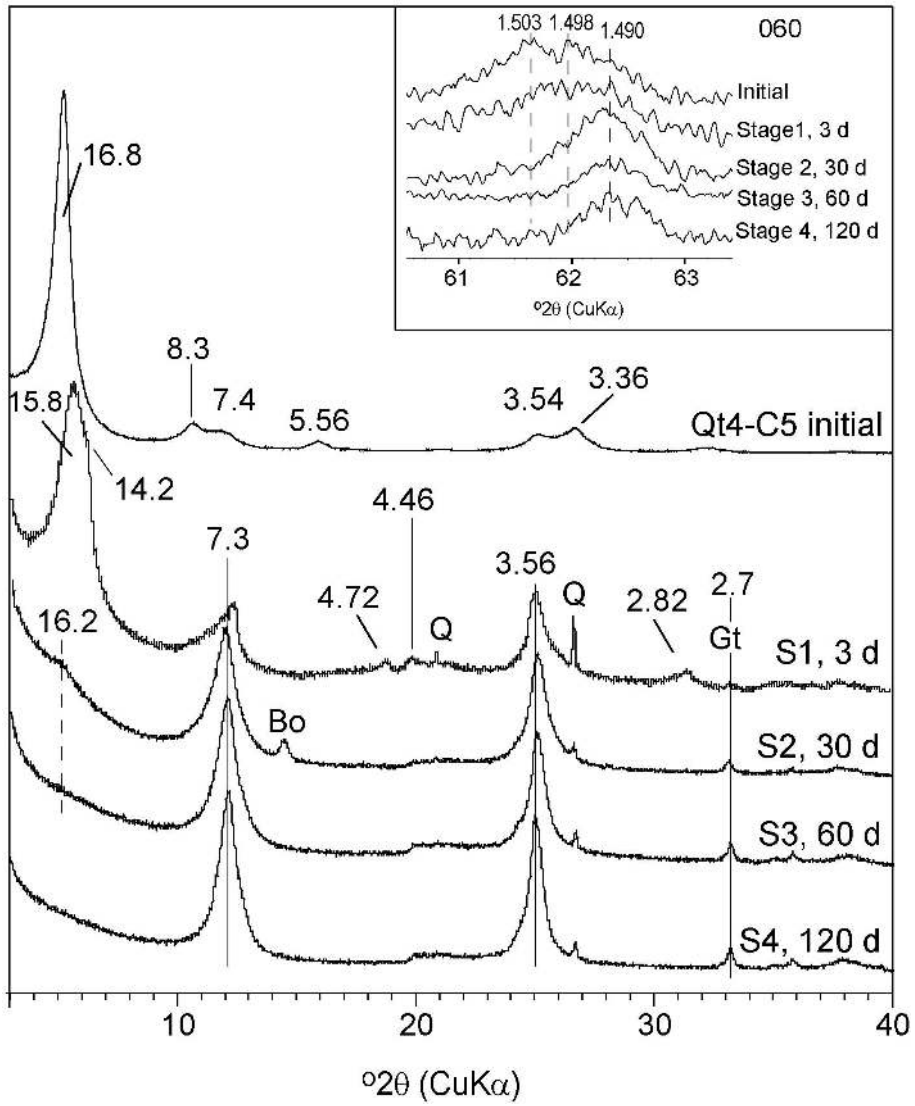

Figure 1. XRD patterns of Fe-beidellite (Qt4-C5 initial) and products of reaction of Fe-beidellite for 3, 30, 60, and 120 days in $AlCl_3$. Patterns in the main window are from oriented, ethylene glycol-solvated powders of the <2 μm fraction, while those in the insert are from randomly oriented <2 μm powders (060 peaks). Peak positions are given in Å. Q is quartz, Bo is boehmite, and Gt is goethite. S1, S2, *etc*. indicate reaction stages as described in the text.

Stage 2, and the 060 region is characterized by a broad peak that spans ~1.50 Å to 1.490 Å centered at 1.497–1.496 Å. At Stage 2 (30 days), the 060 region contained a broad peak centered at 1.492 Å; in Stages 3 and 4 (60 and 120 days, respectively), the 060 peak is centered near end-member kaolinite 060 at 1.490 Å. The occurrence of broad 060 peaks between end-member smectite and kaolinite (rather than separate end-member peaks) from Stages 1, 2, and 3 is consistent with interstratified K-S (Dudek *et al*., 2006). The fact that the 060 peak migrates toward the kaolinite end member with increased reaction time is consistent with increasing % kaolinite layers with time; this is also apparent in the 00*l* data. Goethite was not detected in Qt4-C5 but it occurs in all reaction products and its abundance appears to increase with time as indicated by the intensity of the 2.7 Å peak (note that in Figure 2 the presence of goethite is confirmed by the accompanying peak at 4.17 Å).

Oriented mounts of synthesized clay from Stages 1 and 3 are comparable with pedogenic clays in 10 ka and 125 ka soils from the Costa Rican soil chronosequence (Figure 2) (Fisher and Ryan, 2006; Ryan and Huertas, 2009). These specimens were chosen for comparison because in a broad sense these synthetic clays are mineralogically similar to natural soil clays. Yet while the synthesized clays are broadly similar to interstratified K-S in natural soil clays which increase in % kaolinite with time, some important distinctions are

apparent. First, Al-rich smectite interlayers form as an intermediary in the S → K reaction under synthesized conditions, whereas the natural soil smectites retain some of their expandable interlayers during initial stages of K-S formation. This difference is evident from: (1) the 4.74 Å peak in synthetic K-S produced as a 003 peak of a 14 Å Al-hydroxy 2:1 clay (Figure 1); and (2) incomplete collapse of interlayers in synthesized K-S, even at 400ºC (Figure 2). Second, in contrast to the natural soil clays, no XRD (or TEM) evidence was found for the presence of halloysite in the synthesized clays. This difference is apparent from the different relative intensities of the kaolinite 002 peak (Figure 2) – where halloysite is present (Qt2-B2), the kaolinite 1:1 002 peak is more intense than the 001 peak in the ethylene glycol-solvated state. This behavior is not noted in the synthesized clays (*e.g.* Stage 3 clay), suggesting that the synthesized 1:1 layers are kaolinite rather than halloysite (Hillier and Ryan, 2002).

TEM-AEM

The morphologies and compositions of single crystals from TEM-AEM analysis (Figure 3, Table 1) revealed changes in the composition of the clay mineral assemblage that were consistent with XRD data, indicating S → K-S → K. Initial smectite (Qt4-C5) contained an average of 8% Fe_2O_3 with a range of 5–11% (Table 1); when expressed as molar quantities of atoms per formula unit (a.p.f.u.), the average was 0.36 a.p.f.u. Fe and the range was 0.23–0.50 a.p.f.u. Fe (Figure 4). Based on octahedral Fe content, Qt4-C5 smectites can be subdivided into two groups. Six of the ten original smectite crystals probed from Qt4-C5 contained 5.0–7.2% Fe_2O_3; the remaining four contained 9.3–11.4% Fe_2O_3, suggesting a bimodal population of smectites consisting of relatively Al-rich (Fe-Mg-poor) low-charge smectites (0.27±0.05 a.p.f.u. Fe) and relatively Fe-Mg-rich beidellites (0.47±0.05 a.p.f.u. Fe). Selected structural formulae of these end-members are shown below and mean values are shown in Table 2:

Fe-Mg-rich:
$(Ca_{0.18})(Al_{1.27}Fe_{0.51}Mg_{0.41})(Si_{3.44}Al_{0.56})O_{10}(OH)_2$
Al-rich: $(Ca_{0.09})(Al_{1.58}Fe_{0.27}Mg_{0.13})(Si_{3.98}Al_{0.02})O_{10}(OH)_2$

The Al-rich smectites contain less tetrahedral Al, making them more montmorillonite-like than the Fe-rich smectites, but they are not referred to here as 'montmorillonite' because tetrahedral Al in the Al-rich end-member ranges from 0.02 to, in one case, 0.5 atoms of Al per 4 tetrahedral sites; in contrast, the overall greater tetrahedral Al content (0.3 to 0.6 atoms per four tetrahedral sites) of the Fe-Mg smectites indicates that they are beidellites. To emphasize the differences in octahedral and tetrahedral compositions, these two end-members will be referred to as Al-smectite and Fe-Mg-beidellite. Stage 1 (3 days) clays consist of a mix of smectite, K-S, and discrete Fe-kaolinite crystals. The smectites that occur in the Stage 1 powders are notably

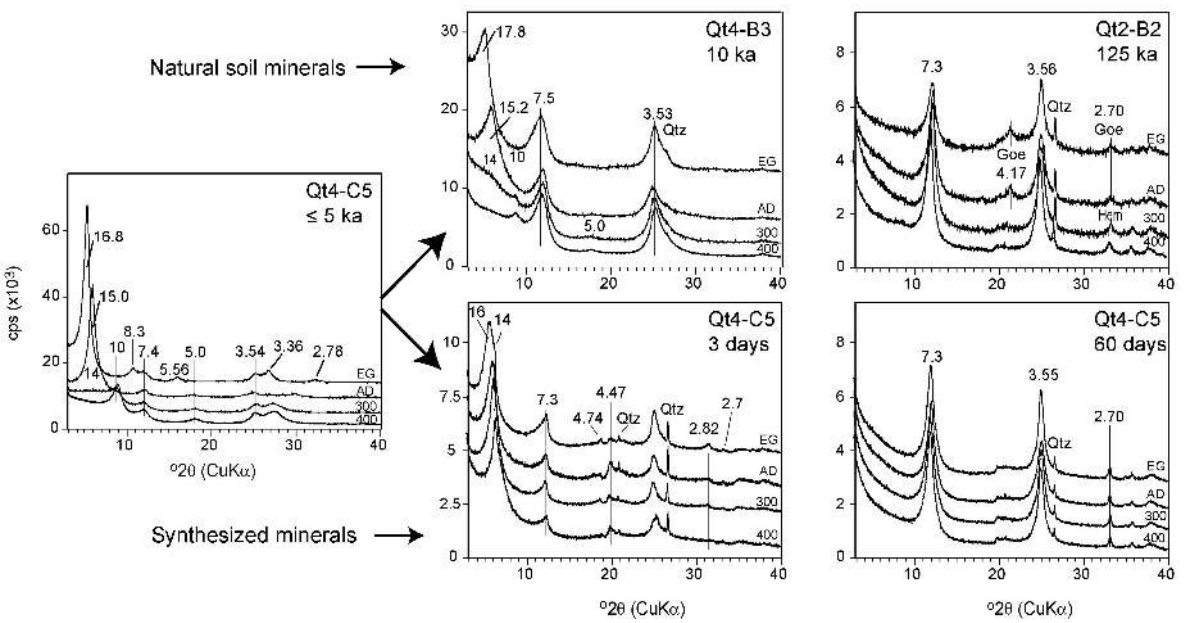

Figure 2. XRD patterns of oriented mounts of representative specimens exposed to ethylene glycol (EG), air dried (AD), and heated to 300 and 400ºC. Peak positions are given in Å. The top row contains natural soil specimens (Ryan and Huertas, 2009), with soil age indicated (ka = 10^3 y). The bottom row contains examples of specimens synthesized from Qt4-C5 after reacting in $AlCl_3$ for 3 days and 60 days which are comparable to the 10 ka and 125 ka natural soil clays, respectively. Note that synthetic K-S (3 days) contains Al-hydroxide interlayers indicated by incomplete expansion with EG and incomplete interlayer collapse with heating.

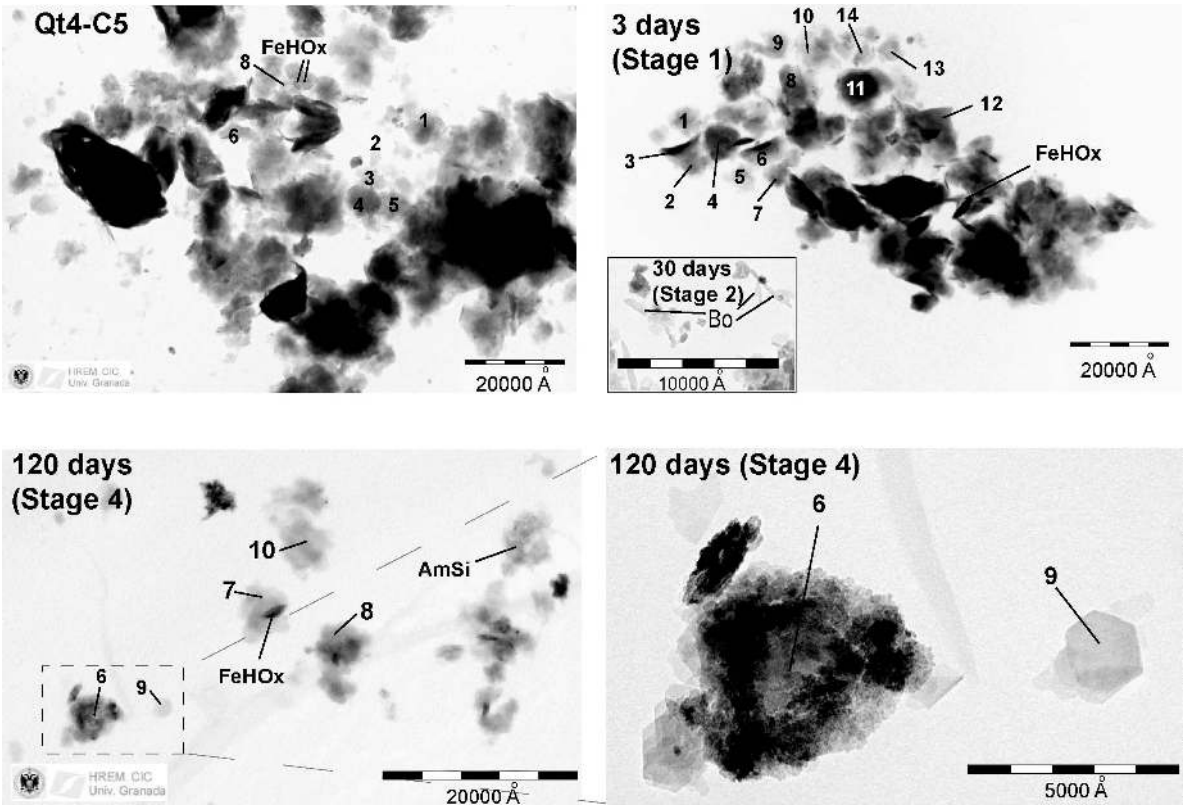

Figure 3. TEM images of single crystals. Tropical soil beidellites (Qt4-C5), kaolinite-smectites, and Fe-kaolinites that dominate the mineral assemblage after 3 days of reaction display platy morphology with some curled edges. The mineral assemblage after 120 days of reaction is dominated by K-S crystals <1 mm in diameter; ~5% of Stage 4 crystals are 0.2 μm in diameter, hexagonal, and in some cases are of end-member $Al_2Si_2O_5(OH)_4$ composition (*e.g.* #9). The inset for Stage 2 depicts bladed boehmite (Bo) crystals detected in many specimens, in this case products of 30 day reaction. Spot AEM compositional analyses are indicated by numerals, values of which are summarized as means in Table 2. Fe oxide or hydroxide is indicated by FeHOx and amorphous silica as AmSi.

Al-rich and are more compositionally similar to the Al-smectites in the initial Qt4-C5 powder than to the Fe-beidellites. Also important to note is that Stage 1 K-S and kaolinite crystals are Fe rich compared to Al-smectites present in the Stage 1 reaction products. Stage 1 Al-smectites contained only 5.1% Fe_2O_3 (0.22 a.p.f.u. Fe_{oct}; range = 0.08−0.32 a.p.f.u. Fe_{oct}). K-S crystals present in Stage 1 reaction products contained an average of 9.6% Fe_2O_3 (0.36 a.p.f.u. Fe_{oct}; range = 0.24−0.52 a.p.f.u. Fe_{oct}) and Stage 1 kaolinite crystals contain an average of 6.9% Fe_2O_3 (0.20 a.p.f.u. Fe_{oct}; range = 0.11−0.29 a.p.f.u. Fe_{oct}). The presence of Al-smectite crystals in Stage 1 products suggests that Al-rich smectite persisted through the first reaction stage; conversely, the absence of Fe-Mg-beidellites in Stage 1 products suggests that this end-member underwent rapid transformation to K-S and Fe-kaolinite. The result is a mineralogical suite in Stage 1 powders that consists of (1) the Al-rich smectite and (2) Fe-Mg-rich K-S and kaolinite with octahedral compositions that reflect the Fe-Mg-rich character of their parent beidellites.

Clays present in Stage 2 powders (30 days) consisted of a mix of Al-smectite, K-S, and Fe-kaolinite, but (1) the proportion of discrete smectite crystals was smaller than in Stage 1 powders and (2) the Fe and Mg concentrations in K-S and kaolinite were smaller than in the Stage 1 powders. Stage 3 powders (60 days) contained no evidence of discrete smectite crystals; apparently all precursor smectite had reacted to K-S and kaolinite by this time. Octahedral Fe and Mg content continued to decrease at the expense of increasing Al (Table 2).

Stage 4 powders are dominated by Fe-bearing kaolinite crystals (only one crystal of K-S was detected) as well as small amounts of ~0.2 μm diameter hexagonal kaolinite crystals with end-member $Al_2Si_2O_5(OH)_4$ composition (Figure 3); these hexagonal kaolinites comprised ~5% of Stage 4 powders. The quantities of Fe_{oct} and Mg_{oct} are smaller in Stage 4 kaolinites than in any precursor smectite, K-S, or Fe-kaolinites (Tables 1 and 2; Figure 4), indicating that Fe and Mg were lost from octahedral sheets as Fe-kaolinite layers recrystallized into more Al-rich compositions toward end-member $Al_2Si_2O_5(OH)_4$.

Table 1. Mean values of chemical compositions of single crystals from AEM analyses expressed as wt.% oxide (anhydrous basis), from soil smectite (Qt4-C5) to products reacted for 3 to 120 days in $AlCl_3$.

	Initial smectite		Kaolinite-smectite		Kaolinite		Clay (total)	
	avg	sd	avg	sd	avg	sd	avg	sd
Qt4-C5	(*N* = 10)						(*N* = 10)	
SiO_2	62.35	4.1	ND	–	ND	–	62.35	4.1
Al_2O_3	25.58	2.6	ND	–	ND	–	25.58	2.6
Fe_2O_3	7.98	2.2	ND	–	ND	–	7.98	2.2
MgO	2.07	1.0	ND	–	ND	–	2.07	1.0
CaO	1.97	0.7	ND	–	ND	–	1.97	0.7
Na_2O	<0.12	–	ND	–	ND	–	<0.12	–
K_2O	<0.12	–	ND	–	ND	–	<0.12	–
Stage 1 (3 days)	(*N* = 5)		(*N* = 8)		(*N* = 7)		(*N* = 20)	
SiO_2	61.82	4.3	53.98	1.9	51.12	2.2	54.94	5.0
Al_2O_3	31.46	2.8	34.36	3.7	39.16	2.4	35.31	4.3
Fe_2O_3	5.06	2.0	9.58	2.4	6.86	2.2	7.50	2.8
MgO	1.43	0.8	1.97	1.7	2.06	1.1	1.87	1.3
CaO	0.21	0.1	0.17	0.2	0.20	0.1	0.19	0.1
Na_2O	<0.12	–	<0.12	–	<0.12	–	<0.12	–
K_2O	0.16	0.1	<0.12	–	0.22	0.3	0.14	0.2
Stage 2 (30 days)	(*N* = 3)		(*N* = 12)		(*N* = 5)		(*N* = 20)	
SiO_2	64.03	2.1	58.43	1.8	53.73	2.1	58.09	3.6
Al_2O_3	29.66	2.9	36.15	2.1	39.38	1.0	35.98	3.5
Fe_2O_3	4.34	0.9	3.53	1.8	4.65	1.0	3.93	1.6
MgO	1.05	0.1	0.88	0.4	0.91	0.4	0.91	0.4
CaO	0.79	0.4	0.67	0.2	1.01	0.4	0.77	0.3
Na_2O	<0.12	–	<0.12	–	<0.12	–	<0.12	–
K_2O	0.12	0.1	0.18	0.3	0.24	0.1	0.19	0.2
Stage 3 (60 days)	(*N* = 0)		(*N* = 11)		(*N* = 7)		(*N* = 18)	
SiO_2ND	–	59.14	2.4	52.69	1.6	56.63	4.3	
Al_2O_3	ND	–	37.13	2.6	42.94	1.4	39.39	4.1
Fe_2O_3	ND	–	2.43	0.8	2.41	0.5	2.42	3.5
MgO	ND	–	0.77	0.3	1.33	0.6	0.99	0.5
CaO	ND	–	0.15	0.1	<0.14	–	0.15	0.2
Na_2O	ND	–	<0.12	–	<0.12	–	<0.12	–
K_2O	ND	–	0.13	0.1	0.20	0.4	0.16	0.2
Stage 4 (120 days)	(*N* = 0)		(*N* = 1)		(*N* = 13)		(*N* = 14)	
SiO_2	ND	–	56.39	–	53.48	1.6	53.69	1.7
Al_2O_3	ND	–	40.58	–	43.94	1.0	43.70	1.3
Fe_2O_3	ND	–	1.99	–	1.04	0.4	1.11	0.4
MgO	ND	–	0.46	–	0.75	0.5	0.73	0.4
CaO	ND	–	0.14	–	<0.14	–	<0.14	–
Na_2O	ND	–	<0.12	–	<0.12	–	<0.12	–
K_2O	ND	–	0.36	–	0.35	0.2	0.35	0.2

ND: not determined

Exchangeable Ca followed a somewhat unpredictable trend – in terms of wt.% oxide in the clay fraction, CaO was 1.97% in Qt4-C5 smectite, dropping to 0.19% in Stage 1 clays and to 0.77% in Stage 2 clays before dropping to 0.15% and <0.14% in Stages 3 and 4. This pattern is attributed here to the formation of boehmite (AlOOH) during Stage 2 (evident in XRD and TEM data, Figures 1, 3). When boehmite crystallized it decreased the availability of Al in reaction solutions and may have diminished the extent of interlayer Al-hydroxy complexes (Figure 2). This would have permitted greater incorporation of Ca into interlayers when clays were saturated with Ca following Stage 2 (relative to Stage 1, where boehmite had not yet formed). Small amounts of Ca in clays from Stages 3 and 4 were caused by the apparent absence of boehmite in these samples and the small abundance of interlayers due to the transformation of S to K.

FTIR

The FTIR spectra of the reaction products indicated mineral structures and compositions which were strik-

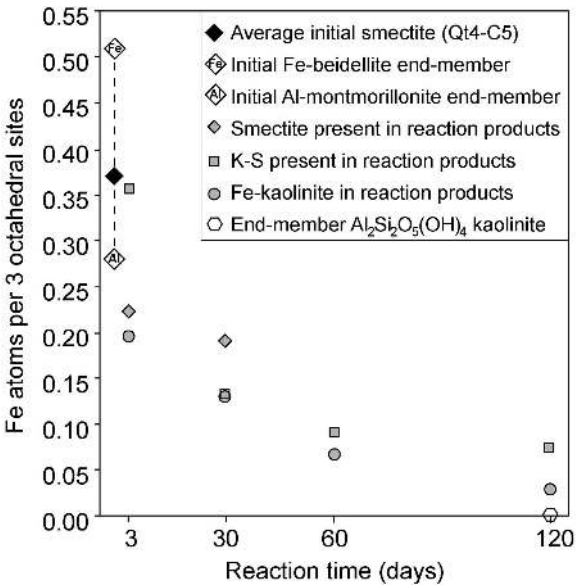

Figure 4. Mean concentrations of Fe in single crystals analyzed by TEM-AEM indicating decrease in octahedral Fe (per unit cell with 3 octahedral sites) with increased reaction time. Note that K-S present after 3 days of reaction is more Fe-rich than smectite still present after 3 days of reaction, and that 3-day smectite is compositionally similar to the Al-smectite end-member in the initial Qt4-C5 smectite sample. Standard deviations are presented in Table 1 as wt.% oxides.

ingly similar to natural soil clays derived from pedogenic smectite Qt4-C5 (Figure 5). The least evolved specimens, including Qt4-C5, the synthesized Stage 1 assemblage (3 days), and the natural soil clay Qt4-B3, exhibited a broad peak at ~3400 cm^{-1} which corresponds to OH-stretching vibrations of adsorbed water, consistent with the abundance of smectite layers in these specimens. The presence of octahedral Fe in smectites, K-S, and early-stage kaolinites was indicated by the Al-OH-Fe bending band at 873 cm^{-1}, and octahedral Mg was suggested by the weak Al-OH-Mg band at ~840 cm^{-1} (Dudek *et al.*, 2007); the weakening and ultimate disappearance of these peaks with increasing reaction time corresponds to decreasing octahedral Fe and Mg with increasing maturity (Figure 5), data which are consistent with TEM-AEM evidence. The trend of decreasing Fe_{oct} and the disappearance of Mg_{oct} seen in the synthesized K-S and kaolinites mimics what is observed in the evolution of S → K-S → K in the natural soil sequence (Ryan and Huertas, 2009).

Peaks at 3698, 3653, and 3622 cm^{-1} are associated with kaolinite (Russell and Fraser 1994); the increase in intensity of these peaks with time is consistent with XRD and TEM-AEM evidence for increasing abundance of kaolinite layers from Stage 1 to Stage 4. The greater intensity of the 3653 cm^{-1} peak in synthesized clays from Stage 3 and Stage 4 (60 and 120 days) indicates that these clays evolved to a greater % kaolinite than the most evolved (125 ka) clay from the natural chronosequence, Qt2-B2 (Ryan and Huertas, 2009).

DTA-TG

The DTA peaks (Figure 6) representing low-temperature (<200ºC) endothermic events are most pronounced in the smectite-dominated Qt4-C5 and correspond to loss of hydration water that is mainly derived from smectite interlayers, released in two stages corresponding to the release of the two hydration shells of Ca in the interlayer at ~100ºC and ~180ºC. These peaks diminished in intensity with increased reaction time, reflecting the

Table 2. Structural formulae (average values) for smectites, K-S, and kaolinites from each stage of the reaction sequence. K-S formulae are presented as an average of 2:1 and 1:1 layers, which allows for comparison of octahedral-sheet compositions among smectite, K-S, and kaolinite.

ID/Stage	Structural formula	Mineral characteristic
Qt4-C5	$Ca_{0.18}(Al_{1.27}Fe_{0.51}Mg_{0.41})(Si_{3.44}\ Al_{0.56})O_{10}(OH)_2$	Initial Fe-beidellite
Qt4-C5	$Ca_{0.09}(Al_{1.63}Fe_{0.28}Mg_{0.13})(Si_{3.82}\ Al_{0.18})O_{10}(OH)_2$	Initial Al-smectite
Qt4-C5	$Ca_{0.13}(Al_{1.51}Fe_{0.37}Mg_{0.19})(Si_{3.72}Al_{0.28})O_{10}(OH)_2$	Initial smectite
Stage 1	$Al_{0.08}(Al_{1.71}Fe_{0.22}Mg_{0.12})(Si_{3.62}Al_{0.38})O_{10}(OH)_2$	Al-smectite
Stage 1	$Al_{0.05}(Al_{1.59}Fe_{0.34}Mg_{0.15})(Si_{2.66}Al_{0.34})O_{7.5}(OH)_3$	K-S
Stage 1	$Ca_{0.08}(Al_{1.73}Fe_{0.20}Mg_{0.12})(Si_{1.96}\ Al_{0.04})O_5(OH)_4$	Fe-kaolinite
Stage 2	$Al_{0.05}\ Ca_{0.05}(Al_{1.76}Fe_{0.19}Mg_{0.09})(Si_{3.76}Al_{0.24})O_{10}(OH)_2$	Al-smectite
Stage 2	$Al_{0.02}Ca_{0.03}(Al_{1.85}Fe_{0.13}Mg_{0.06})(Si_{2.82}Al_{0.18})O_{7.5}(OH)_3$	K-S
Stage 2	$Ca_{0.06}(Al_{1.79}Fe_{0.13}\ Mg_{0.05})Si_{2.0}O_5(OH)_4$	Fe-kaolinite
Stage 3	$Al_{0.03}(Al_{1.91}Fe_{0.07}Mg_{0.07})(Si_{2.83}Al_{0.17})O_{7.5}(OH)_3$	K-S
Stage 3	$(Al_{1.90}\ Fe_{0.07}\ Mg_{0.07})\ Si_{2.0}O_5(OH)_4$	Fe-Mg-kaolinite
Stage 4	$(Al_{1.94}\ Fe_{0.03}\ Mg_{0.04})\ Si_{2.0}O_5(OH)_4$	Platy Fe-Mg-kaolinite
Stage 4	$Al_2Si_2O_5(OH)_4$	Hexagonal kaolinite

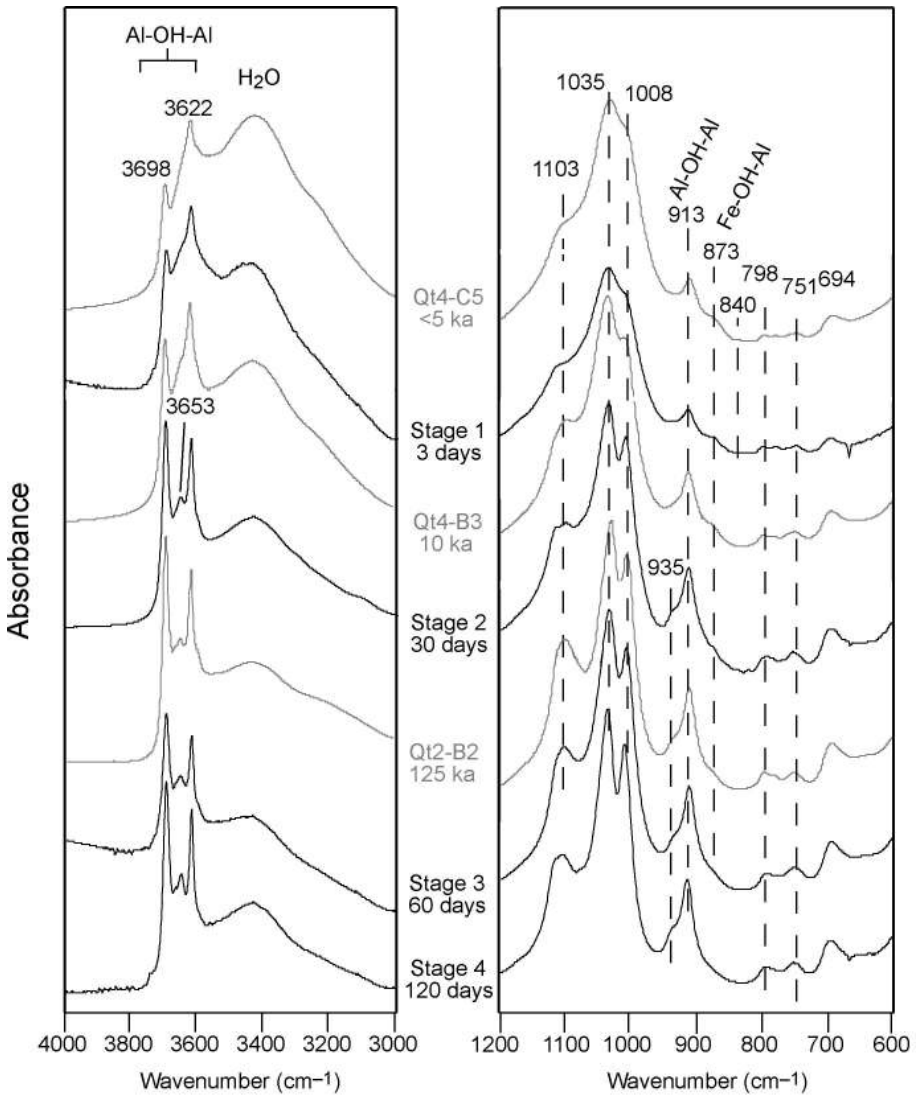

Figure 5. FTIR spectra with OH-stretching region (left) and OH-bending region (right). K-S and kaolinite synthesized from Qt4-C5 are the black traces (reaction times indicated). Natural soil clays (gray traces) are given for reference, including smectite Qt4-C5 and two soil K-S specimens from Ryan and Huertas (2009). Data are presented from minimally evolved smectite-rich (top) to more-evolved, kaolinite-rich (bottom) assemblages. Note that 30 to 60 days of reaction produces an assemblage similar to clays in 125 ka soil. Peak positions are in cm^{-1}.

conversion of smectite to kaolinite. The dominant higher-temperature peaks (>300ºC) correspond to endothermic reactions that range from 502 to 538ºC; these peaks were produced by dehydroxylation of octahedral sheets, and the general shift toward higher temperatures and sharper peaks reflects the increasing abundance of kaolinite in the system. This increase in peak dehydroxylation temperature was caused by increased abundance of Al–OH bonds in the octahedral sheet, where the Al−O octahedral bond (511 kJ/mol) caused dehydroxylation at higher temperature than would be the case for more Fe-Mg-rich octahedral sheets with weaker Fe−O (409 kJ/mol) and Mg−O (362 kJ/mol) bonds (Mackenzie, 1970).

One notable anomaly is the 502ºC peak dehydroxylation in Stage 1 reaction products as compared to the 515ºC peak in initial Qt4-C5 powders. This shift to lower peak dehydroxylation temperature may reflect the presence of newly formed octahedral sheets that were poorly crystallized or partially crystallized and underwent dehydroxylation at a lower temperature than later-stage kaolinites. It could also reflect the disappearance of Fe-beidellites. This is because beidellites and nontronites undergo dehydroxylation at ~550ºC, as compared to *trans*-vacant Al-montmorillonites, which undergo dehydroxylation at ~500ºC (Drits *et al*., 1995). Thus, the initial Qt4-C5 mineral assemblage, consisting of a mixture of Al-montmorillonite and Fe-Mg-beidel-

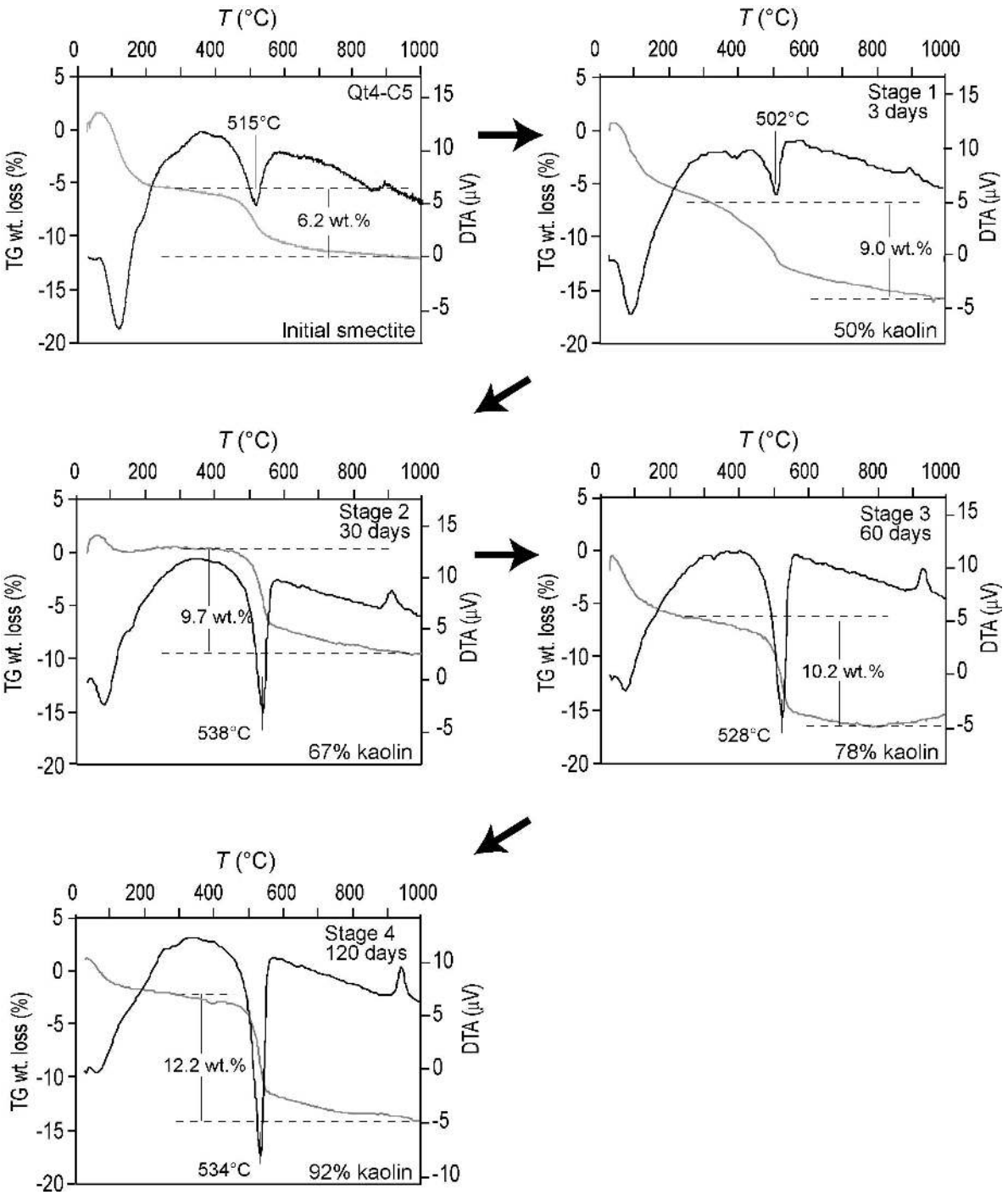

Figure 6. DTA (black) and TG (gray) curves for smectite-rich starting material (top left) and products of reaction in Al-rich solution for 3, 30, 60, and 120 days, respectively. Values used to determine % weight loss caused by dehydroxylation are shown by dashed lines. Peak dehydroxylation temperatures for K-S minerals are also indicated.

lite, produced peak dehydroxylation intermediate to these two end-members, and after the Fe-beidellite had dissolved during Stage 1, the resulting DTA pattern produced a signature more characteristic of Al-smectite. Weak peaks between 250 and 350ºC were probably produced by dehydroxylation of hydroxide minerals, particularly goethite and boehmite (both observed in XRD analysis; Figures 1, 2) as well as by dehydroxylation of gibbsite-like Al-hydroxy-interlayer sheets intercalated with smectite 2:1 layers (Mackenzie, 1970;

Barnhisel and Bertsch, 1989), an observation consistent with XRD evidence.

Qt4-C5 lost 6.2% during dehydroxylation, consistent with nearly pure smectite in the starting mineral powder. Applying the dehydroxylation model of Dudek *et al*. (2006, 2007), Stage 1 powders, with dehydroxylation weight loss of 9.0%, contained approximately equal amounts of smectite and kaolinite layers distributed among Al-smectite, interstratified K-S, and discrete kaolinite (Table 1). Data from DTA-TG (9.7% dehydroxylation weight loss) combined with TEM-AEM and XRD data indicated that Stage 2 powders contained 65−70% K layers, predominantly in K-S and kaolinite; Stage 3 powders (10.2% dehydroxylation weight loss) contained 75−80% K layers in K-S as well as discrete kaolinite; and Stage 4 powders (12.2% dehydroxylation weight loss) contained 90−95% K layers (mainly as discrete Fe-kaolinite and hexagonal kaolinite, with very little remaining interstratified K-S).

Composition of liquid phase

Changes in pH values and cation concentrations of solutions separated from solids at the end of each reaction stage (Table 3) are consistent with XRD, TEM-AEM, and FTIR data. The presence of 3.6−4.3 mmol/L Ca in each post-reaction solution indicates that interlayer Ca was immediately released and replaced by Al hydroxide complexes, an observation consistent with XRD analyses which indicated that Stage 1 smectites contained Al-hydroxy interlayers (indicated by incomplete collapse of smectite interlayers with heating; Figure 2). Concentration of Mg in solution showed a pronounced increase at Stage 2, a finding that is consistent with TEM-AEM data indicating the greatest loss of Mg from octahedral sheets during Stage 2 (Table 2). Rozalen *et al*. (2009) also observed preferential dissolution of Mg-rich octahedral sheets in experimental studies.

The pH of post-reaction solutions (1.0 to 1.2) is appreciably more acidic than the initial pH of 3.4, and this is attributed to the formation of goethite as well as Al-hydroxy interlayers and boehmite (each observed in XRD) and associated deprotonation of water molecules:

$$Fe^{+3} + 2\ H_2O \rightarrow FeOOH + 3H^+$$

$$Al^{+3} + 2\ H_2O \rightarrow AlOOH + 3H^+$$

$$Al^{+3} + 3\ H_2O \rightarrow Al(OH)_3 + 3H^+$$

Goethite crystallization occurs in response to release of iron by dissolution of octahedral sheets; the fixation of Fe into goethite means that Fe present in extracted solutions is not a good proxy for Fe_{oct} liberated during reaction. In fact, none of the concentrations of ions in solution reached the concentrations expected if all released ions had remained in solution. Boehmite presumably crystallized due to a large concentration of Al in the 32 mmol L^{-1} solution. The presence of amorphous silica in TEM analysis of reaction products (Figure 3) indicated that the concentration of silica [H_4SiO_4] in solution underestimated release of Si from tetrahedral sheets. While release of Ca, K, and Mg provides a better proxy for reaction progress, these cations may become adsorbed onto the clays; however, adsorbed cations were not detected in TEM-AEM single-crystal analysis because the standard procedure is to wash powders with Ca^{2+} after separating solids (in order to standardize interlayer occupancy). Thus, the best means available for examining changes to mineral composition in this type of study was to perform direct analyses of single crystals by TEM-AEM (Table 1; Figures 3, 4).

DISCUSSION

Reaction rate and mechanism

Data from multiple analytical approaches indicated that the reaction of smectite to K-S and kaolinite observed in tropical soils (Ryan and Huertas, 2009) can be simulated by experimental alteration of pedogenic smectite. In both the natural soil reaction and in the experimental alteration of S → K-S → K, the reaction rate proceeds logarithmically (Figure 7), where the rate is greatest at the earliest stages and, as is the case with soil reactions, slows progressively with time as the system approaches equilibrium with an acidic solution rich in Al and depleted in Fe, Mg, and base cations.

Given that the greatest disequilibrium between smectite layers (Si-rich tetrahedral sheets and Fe-Mg-bearing octahedral sheets) and the solutions (rich in Al

Table 3. Chemical composition and pH of solutions after hydrothermal experiments run for 3 to 120 days.

Duration, ID	pH	Si (mmol/L)	Al (mmol/L)	Mg (mmol/L)	Fe (mmol/L)	Ca (mmol/L)	K (mmol/L)	Na (mmol/L)
3 days, Stage 1	1.2	1.50	20.31	0.48	0.10	3.62	0.42	0.39
30 days, Stage 2	1.1	3.13	15.26	1.69	0.18	3.44	0.74	0.46
60 days, Stage 3	1.1	3.34	16.27	1.84	0.18	3.88	0.69	0.48
120 days, Stage 4	1.0	5.00	17.67	1.93	0.17	4.32	0.82	0.51

The initial pH of solutions was 3.4

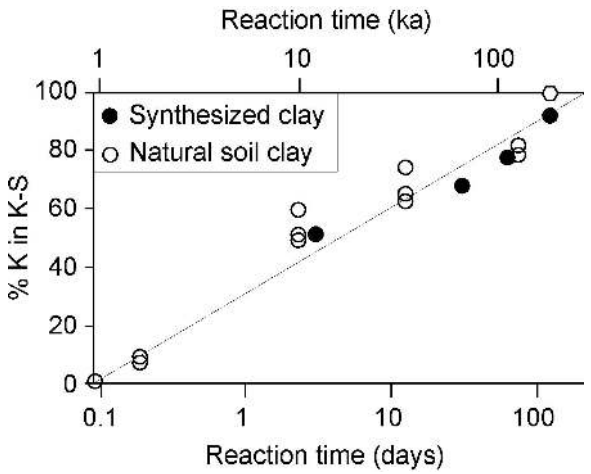

Figure 7. Comparison of reaction rates of smectite to K-S to kaolinite in natural soil clays (from Costa Rica: Fisher and Ryan, 2006; Ryan and Huertas, 2009) relative to synthesized clays (present study). ⎔ indicates the presence of small amounts of hexagonal kaolinite that co-exist with K-S in 120 d (Stage 4) powder.

and H^+ and depleted in Si, Mg, and Fe) occurs in the earliest stages, the reaction rate will be greatest at the earliest stages if the main driving mechanisms are these thermodynamic gradients. The instability of Fe-Mg-bearing octahedral sheets is caused by relatively weak Fe−O bonds (409 kJ/mol) and Mg−O bonds (362 kJ/mol) compared to Al−O bonds (511 kJ/mol) that make octahedral sheets with Fe-Mg prone to hydrolysis in acidic solutions, like those used in this study as well as those in tropical soils. The Al-rich tetrahedral sheets of the Fe-Mg-beidellites may also enhance dissolution relative to the Al-smectites. Thus, Fe-Mg-rich beidellite layers are predicted to decompose and transform to kaolinite layers more rapidly than will Al-smectite layers in this type of system. This is consistent with previous research on smectites, where the initial alteration of volcanic glasses produced Fe-smectite which evolved with time toward Al-smectite (Fiore *et al*., 2001).

After starting with an initial assemblage of two end-member pedogenic smectites (~Fe-Mg-rich beidellites and Al-rich smectites), the mineral assemblage present after 3 days of experimental alteration (Stage 1 powders) no longer contains Fe-Mg-beidellite, and the new assemblage consists of K-S and kaolinite (with similar Fe_{oct} and Mg_{oct} contents to precursor Fe-Mg-beidellite), as well as Al-smectite inherited from initial Qt4-C5 soil clay. The Fe-Mg-rich character of the Stage 1 K-S and kaolinite octahedral sheets imply that they were inherited from the precursor octahedral sheets in Fe-Mg-beidellite layers, a process that was probably influenced by kinetic controls, where rapid crystallization of kaolinite layers following dissolution of Fe-Mg beidellite layers limits diffusion of Fe and Mg out of crystals over the short time span of Stage 1. Previous studies indicated that the reaction of smectite to kaolinite tends to occur laterally within K-S crystallites *via* a cell-preserved, layer-by-layer mechanism (Środoń, 1980; Delvaux *et al*., 1989; Ryan and Huertas, 2009), a process that would tend to foster preservation of precursor octahedral compositions over short time frames where kinetic controls would be favored over thermodynamic controls.

The concentrations of Fe_{oct} and Mg_{oct} in the clay assemblage remained constant during Stage 1; this is attributed to transfer of Fe and Mg from beidellite octahedral sheets to kaolinite octahedral sheets. However, concentrations of Si and Al in the mineral powder changed appreciably during Stage 1. Si decreased by 12% and Al increased by 40%. These changes can be explained stoichiometrically by the reaction mechanisms: (1) tetrahedral stripping (resulting in loss of Si); and (2) tetrahedral inversion paired with growth of new Al-rich octahedral sheets and incorporation of Al-hydroxy complexes into interlayers (Figure 8). Hydrolysis of Fe−O and Mg−O bonds would begin at crystal edges, which in turn would weaken tetrahedral−octahedral bonds and facilitate stripping of tetrahedral sheets. Given their location on crystal faces, tetrahedral sheets (and hence Si) are more easily stripped and transported into solution; conversely, octahedral sheets interior to tetrahedral sheets are more likely to be preserved (or recrystallize *in situ*), at least metastably. This is similar to what was observed by Cuadros *et al*. (2009), who indicated that the initial changes during S → K are tetrahedral stripping followed by adjustments to octahedral sheets (*i.e.* change in octahedral composition).

The stoichiometry of the Stage 1 reaction shown below is consistent with single-crystal compositional analysis by TEM-AEM. In this reaction, two moles of Fe-Mg beidellite react to form three moles of Fe-Mg-bearing kaolinite layers in K-S:

$$2(Ca_{0.15})(Al_{1.3}Fe_{0.5}Mg_{0.4})(Si_{3.5}Al_{0.5})O_{10}(OH)_2 + 1.65\ Al(OH)_3 + 1.25\ H_2O + 0.55\ H^+ \rightarrow 3(Al_{1.55}Fe_{0.33}Mg_{0.27})(Si_{1.8}Al_{0.2})O_5(OH)_4 + 0.3\ Ca^{2+} + 1.6\ SiO_{2(aq)}$$

While all Fe-Mg-beidellite reacts very rapidly (*i.e.* during Stage 1) to Fe-Mg-rich K-S and kaolinite, the trajectory of the Al-montmorillonitic smectites is more gradual. The reaction of Al-smectite to kaolinite reaches its greatest rate at intermediate stages when the system contains randomly interstratified K-S with ~50% of each layer type (Cuadros *et al*., 2009). In this scenario, parts of tetrahedral sheets have been stripped from smectite layers, producing highly unstable kaolinite-like patches that reach their maximum instability at ~50:50 K:S. The rate of transition of Al-smectite to kaolinite can be estimated from DTA and TEM-AEM given the approximately equal proportions of these two end-members in

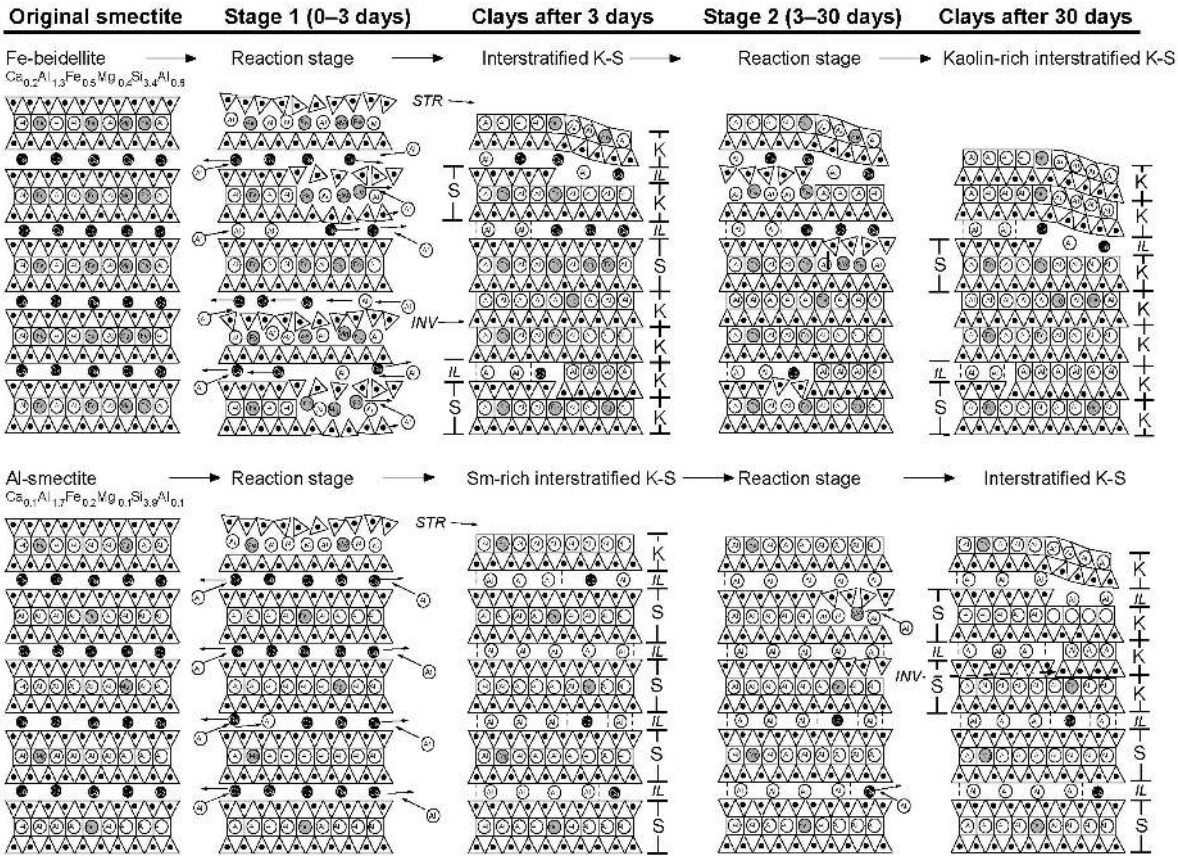

Figure 8. Interpreted reaction mechanisms of smectite layers to kaolinite layers emphasizing apparent differences in reaction rate between Fe-beidellite and Al-smectite end-members. In both examples, smectite layers transform to kaolinite layers laterally within crystals *via* tetrahedral stripping (STR) and tetrahedral inversion (INV). Smectite 2:1 layers and kaolinite 1:1 layers are denoted by S and K, and interlayers by IL, respectively. Black circles represent Ca^{2+} in interlayer sites; the occurrence of Al^{3+} in interlayers is also shown, where much interlayer Al occurs as Al-hydroxy complexes.

initial Qt4-C5, and results indicate that 34% of the Al-smectite end-member reacts to K during Stage 2; an additional 2% undergoes S → K in Stage 3 and another 28% of Al-smectite transforms to K in Stage 4 (Figure 9). By the end of the 120-day experiment, 84% of the Al-smectite end-member had reacted to kaolinite. This observation is very similar to the results of Dudek *et al*. (2007) who found that after 120 days under identical conditions, 86% of Al-montmorillonite had transformed to K, and that the rate of transformation was greatest in intermediate stages.

To summarize the differences in smectite reaction rate and trajectory, Fe-Mg-beidellite reacts to K very rapidly and can be modeled as a logarithmic function with a steep initial slope. Conversely, Al-smectite reacts to K-S or kaolinite slowly in the early stages and then the rate appears to increase exponentially in intermediate stages (Figure 9), followed by a diminished rate of increase in later stages, which effectively represents the type of step function for Al-smectite K-S reactions indicated by Dudek *et al*. (2007) and Cuadros *et al*. (2009). The difference in rate and reaction mechanism of these two smectite end-members is shown schematically in Figure 8.

The hexagonal ~0.2 μm diameter kaolinites with end-member $Al_2Si_2O_5(OH)_4$ composition that appear in the

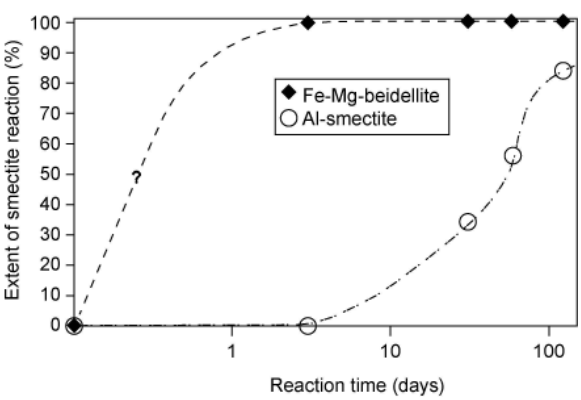

Figure 9. Interpreted differences in reaction rate of Fe-beidellite *vs*. Al-smectite. The symbol '?' indicates uncertainty in the trajectory of the early-stage rapid reaction progress of Fe-beidellite.

mineral assemblage in Stage 4 products (120 days) probably formed *via* dissolution of precursor Fe-Mg-bearing kaolinite followed by neoformation of kaolinite. The reaction of precursor platy Fe-kaolinite to hexagonal kaolinite can be represented as:

$$(Al_{1.73}Fe_{0.20}Mg_{0.12})(Si_{1.96}Al_{0.04})O_5(OH)_4 + 0.23\ Al^{3+} + 0.04\ Si^{4+} \rightarrow Al_2Si_2O_5(OH)_4 + 0.20\ Fe^{3+} + 0.12\ Mg^{2+}$$

This reaction appears to be the only transformation observed in this study that occurs *via* crystal dissolution-precipitation, *i.e*. it does not appear to involve inheritance of precursor tetrahedral or octahedral sheets (or at least parts of pre-existing sheets) within crystallites, as is the case for reaction of smectite to kaolinite layers within K-S crystals. These hexagonal kaolinites are similar in size and morphology to sub-micron kaolinites in Brazilian Oxisols that crystallized from solution following dissolution of precursor sedimentary kaolinites (Muggler *et al*., 2007).

The data obtained in the present study may provide constraints on reaction times required to form hexagonal soil kaolinite. Given that the experimentally altered clays from this study attain the K-S and Fe-kaolinite mineralogy of 120,000 year-old natural clays within 60 days, and that 120 days of experimental alteration are required to form hexagonal, non-Fe-bearing kaolinite, the time required to form incipient Fe-free kaolinite in tropical soils with ~3000 mm MAP and 25ºC MAT probably requires $\geqslant$250,000 y, or in less precise terms, on the order of 10^5 to 10^6 y.

Implications for tropical soils

The experimental alteration of smectite to K-S and eventually to kaolinite in a solution that approximates Al-rich, acidic tropical soil waters (Cornu *et al*., 1997) indicates that this is the expected trajectory of early formed smectite in moist tropical soils. The presence of K-S in tropical soils has been identified infrequently, perhaps because K-S is difficult to recognize in routine analyses, as documented by Wilson (1987), Hughes *et al*. (1993), Cuadros *et al*. (1994), and Środoń (1999). However, given the potential for K-S to retain nutrient cations and sequester Al to a much greater extent than kaolinite, understanding the genetic relationships among smectite, K-S, and kaolinite, as well as the rates and mechanisms of this reaction sequence, especially when trying to predict chemical and mineralogical properties of tropical soils formed on Holocene and late Pleistocene parent material, is critical.

The transformation of pedogenic smectite to a clay assemblage with ~50% K layers (including residual Al-smectite and interstratified K-S) (Figure 7) occurs during Stage 1 (3 days) of experimental alteration and over a 10,000 year span in natural tropical soil (Ryan and Huertas, 2009); however, the subsequent transformation of K-S to Fe-kaolinite and ultimately to hexagonal, non-Fe-bearing kaolinite occurs much more slowly (Figures 4, 9). In experimental alteration, Fe-kaolinite mixed with K-S dominates the assemblage in Stage 3 (60 days) powders, an assemblage which is very similar to the clay mineralogy of 120,000 y old tropical soils (Ryan and Huertas, 2009). Hexagonal non-Fe-bearing kaolinite was only observed in Stage 4 (120 days) powders (as a minority mineral in an assemblage dominated by Fe-kaolinite and K-S), and does not occur in soils of the 120 ka chronosequence (Ryan and Huertas, 2009).

The significance of K-S in tropical soils can be envisioned in two ways. The first is the effect of smectite layers in K-S on soil cation exchange capacity and fixation of aluminum. Considering that plant growth in moist tropical soils is often limited by low concentrations of exchangeable base cations (especially Ca and K) and large amounts of dissolved Al (Korning *et al*., 1994), the persistence of smectite layers in K-S provides a mechanism to retard base cation loss and to enhance sequestration of Al from soil solution. The CEC of natural specimens of tropical soil K-S ranges from 10 to 30 $cmol_c/kg$ (Ryan and Huertas, 2009), a range which is approximately double that of typically reported kaolinite values (*e.g.* Hart *et al*., 2002). The K-S formed by experimental alteration of pedogenic smectite shows a strong capacity for incorporating Al into interlayer spaces, an attribute which has also been observed in naturally occurring K-S (Ryan and Huertas, 2009) and which has been attributed to lowering plant-available Al in tropical soils (Korning *et al*., 1994; Ndayiragije and Delvaux, 2003).

The second impact of the K-S reaction series on tropical soils is the character of the kaolinites (or potentially halloysites) that form *via* transformation of smectite and K-S, particularly regarding the inheritance of Fe (and, in early stages, Mg) in kaolinite octahedral sheets. We attribute the presence of octahedral Fe and Mg in kaolinite to the cell-preserved, layer-by-layer reaction mechanism documented in many previous studies of K-S (*e.g.* Amouric and Olives, 1998; Aspiandar and Eggleton, 2002; Dudek *et al*., 2006, 2007; Ryan and Huertas, 2009). This reaction mechanism may be significant for tropical soils because it could explain the origin of Fe-kaolinites observed in tropical soils by Herbillon *et al*. (1976), Mestdagh *et al*. (1980), Bravard and Righi (1988), Hart *et al.* (2002), and Kanket *et al*. (2005). The occurrence of disordered Fe-kaolinites is probably significant for soil chemistry given that platy, disordered tropical Fe-rich kaolinites have approximately double (4−11 $cmol_c/kg$) the CEC of hexagonal Fe-poor kaolinites (1−5 $cmol_c/kg$) (Hart *et al*. (2002).

ACKNOWLEDGMENTS

This project was supported by funding from the NSF (EAR-1226494), Junta de Andalucía Group RNM-264, and the Whiting Foundation. The authors thank Javier Cifuentes

and Maria del Mar Abad for assistance with TEM and José Maceira Peña for assistance with FTIR and DTA.

REFERENCES

Altschuler, Z.S., Dwornik, E.J., and Kramer, H. (1963) Transformation of montmorillonite to kaolinite during weathering. *Science*, **141**, 148–152.

Amouric, M. and Olives, J. (1998) Transformation mechanisms and interstratification in conversion of smectite to kaolinite; an HRTEM study. *Clays and Clay Minerals*, **46**, 521–527.

Anda, M., Shamshuddin, J., Fauziah, C.I., and Syed Omar, S.R. (2008) Mineralogy and factors controlling charge development of three Oxisols developed from different parent materials. *Geoderma*, **143**, 153–167.

Aspiandar, M.F. and Eggleton, R.E. (2002) Weathering of chlorite: I. Reactions and products in microsystems controlled by the primary mineral. *Clays and Clay Minerals*, **50**, 685–698.

Barnhisel, R.I. and Bertsch, P.M. (1989) Chlorites and hydroxy-interlayered vermiculite and smectite. Pp. 729–788 in: *Minerals in Soil Environments* (2nd edition) (J.B. Dixon and S.B. Weed, editors). Soil Science Society of America, Madison, Wisconsin, USA.

Bravard, S. and Righi, D. (1988) Characteristics of clays in an Oxisol-Spodosol toposequence in Amazonia (Brazil). *Clay Minerals*, **23**, 279–289.

Chadwick, O.A., Derry, L.A., Vitousek, P.M., Huebert, B.J., and Hedin, L.O. (1999) Changing sources of nutrients during four million years of ecosystem development. *Nature*, **397**, 491–497.

Churchman, G.J., Slade, P.G., Self, P.G., and Janik, L.J. (1994) Nature of interstratified kaolin-smectites in some Australian soils. *Australian Journal of Soil Research*, **32**, 805–822.

Cliff, G. and Lorimer, G.W. (1975) The quantitative analysis of thin specimens. *Journal of Microscopy*, **103**, 203–207.

Cornu, S., Ambrosi, J.P., Lucas, Y., and Fevrier, D. (1997) A comparative study of the soil solution chemistry of two Amazonian forest soils (Central Amazonia, Brazil). *Hydrology and Earth System Sciences*, **1**, 313–324.

Cradwick, P.D. and Wilson, M.J. (1972) Calculated X-ray diffraction profiles for interstratified kaolinite-montmorillonite. *Clay Minerals*, **9**, 395–405.

Cuadros, J., Delgado, A., Cardenete, A., Reyes, E., and Linares, J. (1994) Kaolinite/montmorillonite resembles smectite. *Clays and Clay Minerals*, **42**, 643–651.

Cuadros, J., Nieto, F., and Wing-Dudek, T. (2009) Crystal-chemical changes of kaolinite-smectite mixed-layer with progressive kaolinization, as investigated by TEM-AEM and HRTEM. *Clays and Clay Minerals*, **57**, 742–750.

Delvaux, B., Mestdagh, M.M., Vielvoye, L., and Herbillon, A.J. (1989) XRD, IR and ESR study of experimental alteration of Al-nontronite into mixed-layer kaolinite-smectite. *Clay Minerals*, **24**, 617–630.

Delvaux, B., Herbillon, A.J., Vielvoye, L., and Mestdagh, M.M. (1990) Surface properties of clay mineralogy of hydrated halloysitic soil clays. II: Evidence for the presence of halloysite/smectite (H/Sm) mixed-layer clays. *Clay Minerals*, **25**, 141–160.

Drits, V.A., Besson, G., and Muller, F. (1995) An improved model for structural transformations of heat-treated aluminous dioctahedral 2:1 layer silicates. *Clays and Clay Minerals*, **43**, 718–731.

Dudek, T., Cuadros, J., and Fiore, S. (2006) Interstratified kaolinite-smectite: nature of the layers and mechanism of smectite kaolinization. *American Mineralogist*, **91**, 159–170.

Dudek, T., Cuadros, J., and Huertas, F.J. (2007) Structure of mixed-layer kaolinite-smectite and smectite-to-kaolinite transformation mechanism from synthesis experiments. *American Mineralogist*, **92**, 179–192.

Eswaran, H. and de Coninck, F. (1971) Clay mineral formations and transformations in basaltic soils in tropical environments. *Pedologie*, **21**, 181–210.

Etame, J., Gerard, M., Suh, C.E., and Bilong, P. (2009) Halloysite neoformation during the weathering of nephelinitic rocks under humid tropical conditions at Mt Etinde, Cameroon. *Geoderma*, **154**, 59–68.

Fiore, S., Huertas, F.J., Huertas, F., and Linares, J. (2001) Mechanism of smectite formation in volcanic glass as inferred by microscopic (SEM-TEM-AEM) investigation. *Clay Minerals*, **36**, 489–500

Fisher, G.B. and Ryan, P.C. (2006) The smectite to disordered kaolinite transition in a tropical soil chronosequence, Pacific Coast, Costa Rica. *Clays and Clay Minerals*, **54**, 571–586.

Hart, R.D., Gilkes, R.J., Siradz, S., and Singh, B. (2002) The nature of soil kaolins from Indonesia and western Australia. *Clays and Clay Minerals*, **50**, 198–207.

Herbillon, A.J., Mestdagh, M.M., Vielvoye, L., and Derouane, E.G. (1976) Iron in kaolinite with special reference to kaolinite from tropical soils. *Clay Minerals*, **11**, 201–220.

Hillier, S. and Ryan, P.C. (2002) Identification of halloysite (7Å) by ethylene glycol solvation: the 'MacEwan effect'. *Clay Minerals*, **37**, 487–496.

Hong, H., Churchman, G.J., Gu, Y., Yin, K., and Wang, C. (2012) Kaolinite-smectite mixed-layer clays in the Jiujiang red soils and their climate significance. *Geoderma*, **173-174**, 75–83.

Hughes, R.E., Moore, D.M., and Reynolds, R.C., Jr. (1993) The nature, detection and occurrence, and origin of kaolinite/smectite. Pp. 291–323 in: *Kaolin Genesis and Utilization* (H.H. Murray, W.M. Bundy and C.C. Harvey, editors). Special Publication No. **1**, The Clay Minerals Society, Boulder, Colorado.

Kanket, W., Suddhiprakarn, A., Kheoruenromne, I., and Gilkes, R.J. (2005) Chemical and crystallographic properties of kaolin from Ultisols in Thailand. *Clays and Clay Minerals*, **53**, 478–489.

Kantor, W. and Schwertmann, U. (1974) Mineralogy and genesis of clays in red-black toposequences in Kenya. *Journal of Soil Science*, **25**, 67–78.

Korning, J., Thomsen, K., Dalsgaard, K., and Nørnberg, P. (1994) Characters of three udults and their relevance to the composition and structure of virgin rain forest of Amazonian Ecuador. *Geoderma*, **63**, 145–164.

Mackenzie, R.C. (1970) Simple phyllosilicates based on gibbsite- and brucite-like sheets. Pp. 498-537 in: *Differential Thermal Analysis* (R.C. Mackenzie, editor). Academic Press, London.

Mestdagh, M.M., Vielvoye, L., and Herbillon, A.J. (1980) Iron in kaolinite: II. The relationship between kaolinite crystallinity and iron content. *Clay Minerals*, **15**, 1–13.

Moore, D.M. and Reynolds, R.C. Jr. (1997) Identification of mixed-layer minerals. Pp. 261–297 in: *X-ray Diffraction and the Identification and Analysis of Clay Minerals* (D.M. Moore and R.C. Reynolds, editors). Oxford University Press, New York.

Muggler, C.C., Buurman, P., and van Doesburg, J.D.J. (2007) Weathering trends and parent material characteristics of polygenetic oxisols from Minas Gerais, Brazil: I. Mineralogy. *Geoderma*, **138**, 39–48.

NAP (National Academy Press) (1982) *Ecological Aspects of Development in the Humid Tropics*. National Academy Press, Washington D.C.

Ndayiragije, S. and Delvaux, B. (2003) Coexistence of allophone, gibbsite, kaolinite and hydroxy-Al-interlayered 2:1 clay minerals in a perudic Andosol. *Geoderma*, **117**, 203–214.

Petschick, R. (2000) *MacDiff*. http://www.ccp14.ac.uk/ccp/ccp14/ftp-mirror/krumm/Software/macintosh/macdiff/MacDiff.html. Accessed 18 July 2008.

Quantin, P., Balesdent, J., Bouleau, A., Delaune, M., and Feller, C. (1991) Premiers stades d'altèration de ponces volcaniques en climat tropical humide (Montagne Pelèe, Martinique). *Geoderma*, **50**, 125–148.

Righi, D., Terribile, F., and Petit, S. (1999) Pedogenic formation of kaolinite-smectite mixed layers in a soil toposequence developed from basaltic parent material in Sardinia (Italy). *Clays and Clay Minerals*, **47**, 505–514.

Rozalén, M.L., Huertas, F.J., and Brady, P.V. (2009) Experimental study of the effect of pH and temperature on the kinetics of montmorillonite dissolution. *Geochimica et Cosmochimica Acta*, **73**, 3752–3766.

Russell, J.D. and Fraser, A.R. (1994) Infrared methods. Pp. 11–67 in: *Clay Mineralogy: Spectroscopic and Chemical Determinative Methods* (M.J. Wilson, editor). Chapman & Hall, London.

Ryan, P.C. and Huertas, F.J. (2009) The temporal evolution of pedogenic Fe-smectite to Fe-kaolin *via* interstratified kaolin-smectite in a moist tropical soil chronosequence. *Geoderma*, **151**, 1–15.

Środoń, J. (1980) Synthesis of mixed-layer kaolinite/smectite. *Clays and Clay Minerals*, **26**, 419–424.

Środoń, J. (1999) Nature of mixed-layer clays and mechanisms of their formation and alteration. *Annual Review of Earth and Planetary Sciences*, **27**, 19–53.

Thanachit, S., Suddhiprakarn, A., Kheoruenromne, I., and Gilkes, R.J. (2006) The geochemistry of soils on a catena on basalt at Khon Buri, northeast Thailand. *Geoderma*, **135**, 81–96.

Vitousek, P.M. and Sanford, R.L., Jr. (1986) Nutrient cycling in moist tropical forest. *Annual Review of Ecological Systematics*, **17**, 137–167.

Wada, K., Kakuto, Y., and Ikawa, H. (1990) Clay minerals of two Eutrandepts of Hawaii, having isohyperthermie temperature and ustic moisture regimes. *Soil Science Society of America Journal*, **54**, 1173–1178.

Wilson, M.J. (1987) Soil smectites and related interstratified minerals: recent developments. Pp. 167–173 in: *Proceedings of the International Clay Conference, Denver* (L.G. Schultz., H. van Olphen and F. Mumpton, editors). The Clay Minerals Society, Colorado, USA.

(*Received 21 April 2013; revised 23 July 2013; Ms. 763; AE: M. Kawano*)